IMECE2025-166672

FINITE ELEMENT MODELING OF FIXED-FIXED BEAMS UNDER SHOCK EXCITATION WITH ACTIVE CONTROL

Trotter Roberts¹, Mohsen Gol Zardian¹, Joud N. Satme¹, Austin R.J. Downey^{1,2}

¹Department of Mechanical Engineering, University of South Carolina, Columbia, SC 29208 ²Department of Civil and Environmental Engineering, University of South Carolina, Columbia, SC 29208

ABSTRACT

Effective vibration suppression is vital to ensure the structural integrity of dynamically loaded systems in aerospace, automotive, and manufacturing systems. High-rate dynamic disturbances, such as shocks, impacts, and rapid load changes, produce short-duration, large-magnitude responses that overwhelm conventional damping approaches. Transient dynamics are characterized by non-stationary behavior, model uncertainty, and random variability of external forces, requiring control systems to respond quickly with flexibility. While passive damping systems are very effective in steady-state regimes, they lack responsiveness to handle impulsive disturbances. Active vibration control, on the other hand, offers real-time adjustability in the form of feedback mechanisms to alter structural response on submillisecond timescales. In this paper, a model built using the finite element method (FEM) of an impulse-loaded fixed-fixed beam is developed to approximate experimental conditions representative of shock-excited printed circuit boards subjected to drop tower impact. The beam is modeled using a modified Euler-Bernoulli beam theory, where axial degrees of freedom are incorporated alongside conventional transverse and rotational DOFs at each node. This extension enables the simulation of axial loading effects arising from actuator forces, which are axially applied in real-world implementations to induce bending moments. Surface-mounted control actuators are introduced as in-plane force inputs that generate localized moment effects, thereby emulating the behavior of piezoelectric bending actuators. While no direct axial forces are applied as part of the control strategy, the model captures the resulting axial stress distributions and associated geometric stiffening effects implicitly through its structural formulation, while Rayleigh damping and Newmark-Beta time integration schemes are used to simulate transient dynamics. A mesh convergence test confirms model validity under steady-state conditions, and time-domain simulations demonstrate vibration reduction through moment-based actuation. The focus of the work is the enhancement of FEM formulation to accurately describe beam response under dynamic loading and the creation

of a computational foundation for evaluating active control techniques. Simulations demonstrate notable reductions in peak displacement and settling time when control forces are activated. This study lays the groundwork for robust, simulation-driven vibration control in high-rate dynamic environments.

Keywords: vibration control, finite element modeling, structural dynamics, active damping, machine learning

1. INTRODUCTION

High-rate dynamic environments, such as those encountered in aerospace, defense, and advanced manufacturing systems, subject structures to shock loads and high-G events occurring over extremely short durations, often in the microsecond to millisecond range. These conditions result in large stress gradients, abrupt deformations, and limited time for mitigation, posing a significant challenge for conventional control and monitoring systems. Passive damping solutions like viscoelastic layers and tuned mass dampers are generally insufficient in these regimes due to their fixed response rates and inability to adapt in real time [1]. Effective mitigation under such conditions requires control strategies capable of extremely fast sensing, computation, and actuation. As highlighted by Dodson et al. [2], traditional structural health monitoring frameworks struggle to meet these demands due to bandwidth constraints and latency in decisionmaking processes. Their work emphasizes the need for reducedorder models, low-latency actuation, and adaptive algorithms that can function within the brief windows available during high-rate events. Motivated by these challenges, the present study explores moment-based control using localized rotational actuation, providing a physically implementable and computationally efficient mechanism for suppressing vibrations under extreme transient conditions.

Active vibration control techniques address the limitations of passive systems by applying real-time corrective forces, making them particularly suited for shock loading, where abrupt, high-magnitude forces over short durations require rapid sensing and actuation to suppress structural response before damage occurs.

Among the techniques, the use of smart materials, particularly piezoelectric actuators, has gained popularity due to their high electromechanical response and compact size [3]. Piezoelectric actuators generate axial strains under applied electric fields, and when bonded eccentrically to a structure, these axial strains manifest as bending moments on the beam. This coupling effect makes them highly effective for controlling both axial and flexural vibrations in beam-like structures [4].

To adequately represent such systems in a numerical framework, a high-fidelity finite element model is required. In this case, a model of the beam using FEM was developed to incorporate both axial and bending responses within each element. The stiffness matrix was developed to have contributions from axial deformation, described via linear Lagrange shape functions, and bending deformation, described via cubic Hermite function [5].

The FEM framework was developed to simulate the influence of control actions made by piezoelectric actuators, producing in-plane actuating forces but manifested as bending forces. The moments are introduced through the application of opposing torques at neighboring rotational degrees of freedom, simulating effectively the eccentric action of a surface-bonded actuator [6, 7]. The outcome is a control-augmented beam model that can capture both the distributed mass and stiffness properties of the structure and the localized nature of actuator inputs.

The model also includes boundary conditions appropriate to practical mounting arrangements. Specifically, a fixed–fixed beam arrangement was employed to represent structural constraints common in embedded systems, circuit boards, aerospace panels, and mechanical subassemblies [8]. These constraints largely dictate natural frequencies and mode shapes, and thus their accurate representation is key to predictive modeling and control synthesis [9].

This study introduces a simulation-based framework for active vibration control of fixed-fixed beams under shock loading using moment-based actuation. The finite element model incorporates rotational degrees of freedom to apply control moments, mimicking the mechanical behavior of surface-mounted piezoelectric devices. A curvature-sensitive PID controller is embedded directly into the time-domain solver to enable real-time suppression of transient oscillations. Example codes associated with this work are available through a public repository [10]. The contributions of this work are twofold. First, it presents a finite element implementation of moment-based actuation via rotational DOFs for realistic modeling of piezoelectric-like control. Second, it demonstrates a real-time PID control strategy tailored for high-rate shock environments. The framework is validated through both static and dynamic benchmarks on a beam representative of FR4 circuit boards, laying the groundwork for future experimental and data-driven control development.

2. BACKGROUND

This work builds on recent experimental studies that characterize the response of electronic assemblies to high-rate shock loading, particularly in the context of structural health monitoring and active control. Printed circuit boards (PCBs) constructed from FR4 composite have been used in drop tower experiments to simulate the effects of impulsive loads in constrained geome-

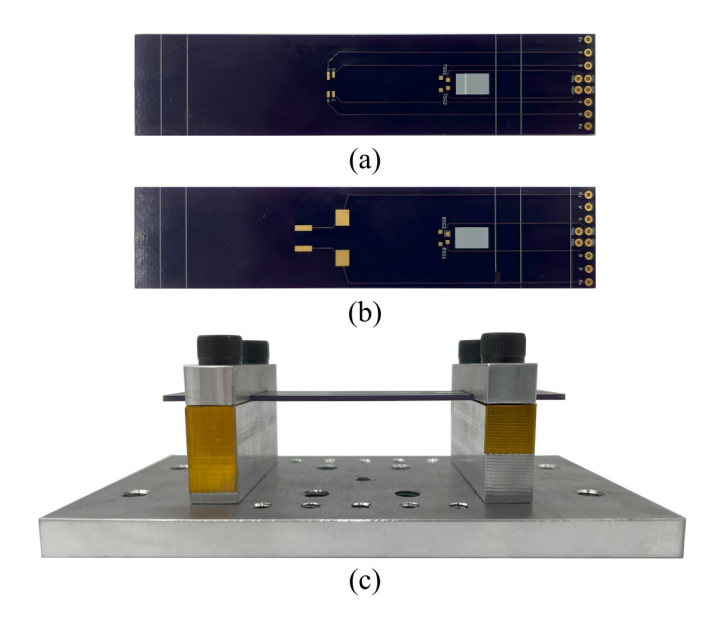


FIGURE 1: REPRESENTATIVE FR4 PCB BEAM: (A) TOP VIEW, (B) BOTTOM VIEW, AND (C) FIXED-FIXED MOUNTING ARRANGEMENT USED IN DROP TOWER TESTING.

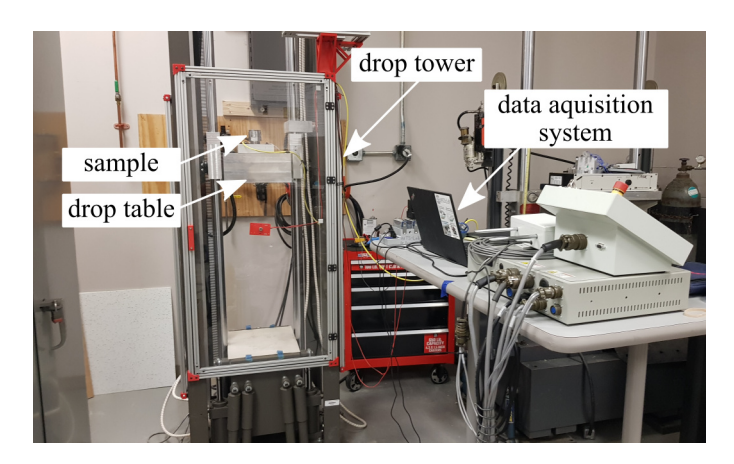


FIGURE 2: DROP TOWER SYSTEM USED TO APPLY VERTICAL IMPULSIVE LOADS TO PCB TEST STRUCTURES WITH KEY COMPONENTS ANNOTATED.

tries. As shown in Figures 1 and 2, test configurations typically employ fixed–fixed boundary conditions with controlled vertical impacts to replicate shock-like mechanical environments. These setups provide a repeatable platform for evaluating embedded sensing and actuation strategies under high-G excitation. Yount et al. [11] demonstrated the utility of this testbed for vibration-based damage detection using onboard signal processing and frequency tracking. Complementary to this, Roberts et al. [9] employed finite element modeling to match experimental conditions and investigate actuator placement and control strategies for suppressing transient deformation. The present study adopts a similar beam configuration and material assumptions to emulate these physical conditions in simulation, enabling the investigation of curvature-sensitive control laws and moment-based actuation for shock mitigation.

TABLE 1: SIMULATED BEAM GEOMETRY AND MATERIAL PROP-ERTIES APPROXIMATING FR4 PCB.

width	thickness	length	
25.40 mm	1.60 mm	88.90 mm	
density	Young's modulus		
1900 kg/m ³	18.60 GPa		

3. METHODOLOGY

This study develops a finite element model to simulate the dynamic behavior of a fixed-fixed beam subjected to shock loading. The model captures both axial and transverse dynamics and integrates moment-based actuation to reflect the behavior of surface-mounted control devices such as piezoelectric patches. These capabilities enable the beam model to replicate realistic conditions in structural systems subjected to shock loads, such as in aerospace, electronics, or mechanical structures [5, 12]. In particular, the simulated beam geometry and material properties were selected to approximate a 175 Tg FR4 composite PCB, a widely used substrate material in electronics. The simulated beam is discretized into 50 nodes with 49 finite elements, each possessing axial, vertical, and rotational degrees of freedom. Table 1 summarizes the updated material and geometric parameters.

3.1. Finite Element Formulation

The finite element model employs a one-dimensional (1D) Euler-Bernoulli beam formulation capable of capturing axial, transverse, and rotational effects, which are critical in systems utilizing piezoelectric actuators. These actuators typically apply axial forces, which, due to their placement, generate bending moments that contribute to vibration suppression. The beam's displacement is approximated using shape functions, and the resulting stiffness and mass matrices are computed for each element. Although the beam is modeled with degrees of freedom in both the axial and transverse directions, it remains a 1D Euler-Bernoulli beam formulation. Each node is assigned three degrees of freedom: axial displacement, vertical displacement, and rotation. This configuration enables the simulation of two-dimensional (2D) structural behavior while maintaining computational efficiency associated with 1D elements.

To accurately model real-world systems, the finite element model was updated to include the coupling between axial forces and bending behavior. Axial stiffness influences the overall beam dynamics, which, in combination with bending stiffness, impacts the system's response under dynamic loads. In-plane control forces, applied through piezoelectric actuators (modeled as moments), were incorporated to better simulate the effect of these actuators, which are commonly used in practical applications to suppress vibrations [13].

The governing equation for the beam, considering both axial and bending forces, in its strong form is expressed as:

$$EI\frac{\partial^4 w}{\partial x^4}(x,t) + N\frac{\partial^2 w}{\partial x^2}(x,t) + \rho A\frac{\partial^2 w}{\partial t^2}(x,t) = 0, \qquad (1)$$

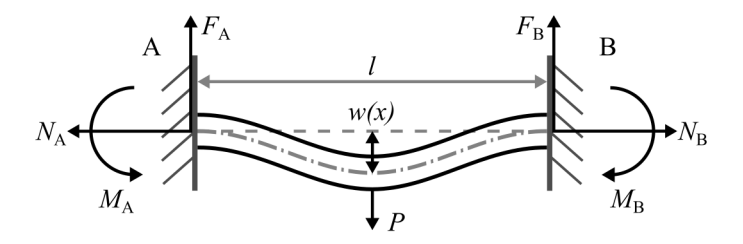


FIGURE 3: AN ILLUSTRATION DEPICTING THE FREE BODY DIAGRAM OF A FIXED-FIXED BEAM SUBJECTED TO A TRANSVERSE POINT LOAD.

where w(x,t) is the transverse displacement, E is Young's modulus, I is the beam's moment of inertia, N is the axial force, ρ is the material density, and A is the beam's cross-sectional area. This equation governs the behavior of the beam and is solved numerically using the FEM to approximate the displacement, velocity, and acceleration at each node along the beam.

Figure 3 depicts the modeled beam, which is fixed at both ends and loaded transversely at its center by a point force P, also termed F_{impact} , resulting in internal axial forces N_A , N_B , bending moments M_A , M_B , and vertical reaction forces F_A , F_B .

In the FEM, the displacement field w(x,t) of the beam is approximated as a sum of shape functions $\phi_j(x)$ multiplied by time-dependent nodal values $w_j(t)$. The displacement at any point along the beam is given by:

$$W(x,t) = \begin{bmatrix} u(x,t) \\ w(x,t) \end{bmatrix} = \sum_{j=1}^{N} \begin{bmatrix} u_j(t) \phi_j(x) \\ w_j(t) \psi_j(x) \end{bmatrix}, \tag{2}$$

where $\phi_j(x)$ and $\psi_j(x)$ are the shape functions associated with axial and transverse displacements, respectively. These shape functions define how displacement varies spatially within each finite element, ensuring appropriate continuity and interpolation between nodes. The coefficients $u_j(t)$ and $w_j(t)$ represent the nodal degrees of freedom, which are the values of axial and transverse displacement at the finite element nodes as functions of time. This formulation allows the continuous displacement field of the beam to be approximated by a finite set of time-dependent variables.

For an element of length l, the shape functions and corresponding nodal degrees of freedom are defined as:

$$W_{e} = \begin{bmatrix} u_1 & w_1 & \theta_1 & u_2 & w_2 & \theta_2 \end{bmatrix}^{T}, \tag{3}$$

where u_1, u_2 are axial displacements, w_1, w_2 are vertical displacements, and θ_1, θ_2 are rotational displacements at the two element nodes. These degrees of freedom and their physical interpretation are illustrated in Figure 4. The inclusion of rotational degrees of freedom is essential for Euler-Bernoulli beam elements, as it allows the model to represent curvature continuity and apply bending moments. In this study, these DOFs enable the simulation of moment-based actuation by applying torques directly to node rotations.

For each beam element, both a stiffness matrix and a mass matrix are assembled to model its structural behavior under loading. The stiffness matrix captures the element's resistance to

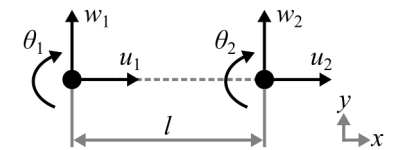


FIGURE 4: AN ILLUSTRATION DEPICTING THE DEGREES OF FREEDOM AND INTERNAL FORCES FOR A 1D BEAM FINITE ELEMENT.

deformation due to both axial and bending effects. The displacement vector for each element is defined $W_{\rm e}$ (eq. 3). The element stiffness matrix is formed by summing the contributions from axial and bending responses:

$$K_{ij}^{(e)} = \int_0^h EA \,\phi_i'(x)\phi_j'(x) \,dx + \int_0^h EI \,\psi_i''(x)\psi_j''(x) \,dx, \quad (4)$$

where $\phi_i(x)$ are the linear Lagrange shape functions used for axial deformation and $\psi_i(x)$ are the cubic Hermite shape functions used for bending deformation. Both shape functions are defined over the reference coordinate $\xi = x/h \in [0,1]$. The Hermite shape functions ensure C^1 continuity of the transverse displacement field, which is essential for satisfying the continuity of slope and bending moment across element boundaries in Euler-Bernoulli beam theory [14].

The element mass matrix accounts for the inertia associated with both axial and transverse motion. A consistent mass matrix formulation is employed here, which arises directly from integrating the shape functions and preserves dynamic coupling. This approach ensures more accurate inertia representation, especially under high-rate loading, compared to lumped mass approximations [15]. It is computed by integrating the shape functions over the element length:

$$M_{ij}^{(e)} = \int_0^h \rho A \,\phi_i(x)\phi_j(x) \,dx + \int_0^h \rho A \,\psi_i(x)\psi_j(x) \,dx. \tag{5}$$

These matrices are assembled globally for the entire beam, representing the full dynamic system.

Boundary conditions are applied to simulate a fixed-fixed beam, where the displacement and rotation at both ends are constrained (as shown in Figure 1). This approach enforces Dirichlet boundary conditions by zeroing the corresponding rows and columns in the global matrices and setting the diagonal to unity [16]. An example of the beam discretization and boundary constraints is illustrated in Figure 5.

The beam's equation of motion is discretized to approximate the system's dynamic behavior. The discretized equation of motion is expressed as:

$$M\ddot{W} + C\dot{W} + KW = F(t), \tag{6}$$

where M is the mass matrix, C is the damping matrix, K is the stiffness matrix, and F(t) represents the applied external forces. The total external force vector is defined as:

$$F(t) = F_{\text{impact}}(t) + F_{\text{control}}(t), \tag{7}$$

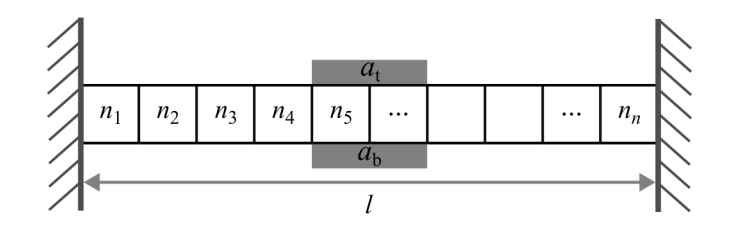


FIGURE 5: AN ILLUSTRATION DEPICTING THE DISCRETIZATION OF THE FIXED-FIXED BEAM.

where $F_{\rm impact}(t)$ represents an externally applied disturbance, and $F_{\rm control}(t)$ is the time-varying actuation computed by the controller. Both simulations used identical loading conditions: a 30 N rectangular force applied vertically at the midpoint node for 0.1 milliseconds, beginning at t = 0.005 seconds. This profile mimics a short-duration shock load, as encountered in drop testing or blast scenarios [17].

The damping matrix *C* was constructed using the Rayleigh damping model, which expresses damping as a linear combination of the mass and stiffness matrices:

$$C = \alpha M + \beta K,\tag{8}$$

where α and β are the mass and stiffness proportional damping coefficients, respectively. These coefficients were computed to yield a 2% critical damping ratio for the first two natural frequencies of the beam. The undamped modal frequencies were obtained from eigenvalue analysis of the reduced stiffness and mass matrices, and the values of $\alpha=65.53$ and $\beta=3.95\times10^{-6}$ were calculated to yield a 2% critical damping ratio for the first two natural frequencies. This was done by solving a system of two equations that relate the modal damping ratio to the Rayleigh parameters and the corresponding modal frequencies. This method provides a practical approximation commonly used in structural dynamics, as it maintains low damping in higher modes while introducing modal energy dissipation in the dominant vibration modes [12, 18].

To integrate the system's behavior over time, the Newmark-Beta time integration method is employed. This method provides a stable numerical solution for dynamic systems. The time integration is defined as:

$$W_{n+1} = W_n + \dot{W}_n \Delta t + \frac{1}{2} \ddot{W}_n \Delta t^2, \tag{9}$$

where Δt is the time step, and W_n , \dot{W}_n , and \ddot{W}_n are the displacement, velocity, and acceleration at the current time step n. Using this approach, the system is updated according to the following equation:

$$\left(K + \frac{\gamma}{\beta \Delta t}C + \frac{1}{\beta \Delta t^2}M\right)W_{n+1} = F_{n+1} + \text{previous terms.} \quad (10)$$

where $\gamma = 0.5$, $\beta = 0.25$, and $\Delta t = 0.1$ milliseconds are the standard Newmark parameters. This implicit time integration scheme ensures numerical stability and allows accurate prediction of the beam's transient response at each time step, taking into account the system's inertia, damping, and stiffness.

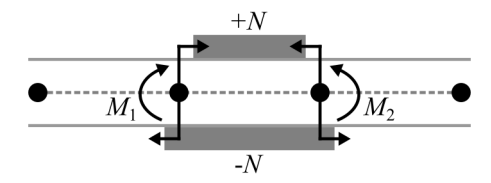


FIGURE 6: AN ILLUSTRATION DEPICTING THE CONTROL FORCE AND GENERATED MOMENTS APPLIED AT THE CONTROL NODE.

3.2. Control Implementation

This study simulates the effect of active bending moment actuation, motivated by the mechanical influence of piezoelectric patches bonded to the upper and lower surfaces of a beam. While the electromechanical behavior of such actuators is fundamentally three-dimensional, their primary mechanical contribution—imposing opposing torques due to off-midline placement—can be effectively approximated in a one-dimensional finite element model by applying a discrete moment couple at adjacent beam nodes.

In this implementation, each actuator is centered between two nodes along the beam. Rather than applying axial forces, the control force $F_{\rm control}$ computed by the controller is converted into an equivalent moment couple and applied directly to the rotational degrees of freedom at the selected control nodes. The resulting moment is calculated as:

$$M_{\text{control}} = F_{\text{control}} \cdot \frac{h}{2},$$
 (11)

where h is the thickness of the beam, and h/2 is the vertical offset between the actuator and the beam's mid-line. This expression reflects the moment generated by a force couple acting through an arm equal to half the beam thickness. This formulation arises from treating the actuator force as a couple acting over a lever arm equal to half the beam thickness, consistent with the behavior of symmetric piezoelectric patches on top and bottom surfaces [19, 20].

The torque $M_{\rm control}$ is applied as equal and opposite moments at the two adjacent nodes spanning the actuator. This generates a localized bending effect consistent with the physical behavior of real actuators. The value of $F_{\rm control}$ is updated at each time step by an external control algorithm, which determines the required actuation based on the beam's dynamic state (e.g., displacement, velocity, or acceleration). This control force is not derived intrinsically from the finite element model but is instead treated as an external input applied to the system. Within the FEM context, only the in situ application of the force is considered i.e. as a moment couple at adjacent nodes, and added to the global force vector at each integration step.

These control moments are assembled into the system's global force vector through their contributions to the rotational degrees of freedom at the control nodes. They are then integrated into the governing equations of motion (eq. 6) and updated at each time step using the numerical integration scheme (eq. 10). Figure 6 illustrates the placement of the control nodes and the moment application along the beam.

The proportional-integral-derivative controller applies a time-varying moment couple to the rotational degrees of freedom at nodes 16 and 34. These nodes were selected to span the central region of the beam, where curvature is highest during midspan deflection. The control law is formulated using feedback from both the relative rotation and angular velocity between these nodes:

$$M_{\text{control}} = -K_p \,\Delta\theta - K_d \,\Delta\dot{\theta} - K_i \int \Delta\theta \,dt,\tag{12}$$

where $\Delta\theta = \theta_R - \theta_L$ is the relative rotation between the right and left control nodes, and $\Delta\dot{\theta} = \dot{\theta}_R - \dot{\theta}_L$ is the relative angular velocity. The final term integrates the curvature difference over time to accumulate persistent deflection error. The proportional gain $K_p = 0.25$ was chosen to provide restorative action based on curvature, while the derivative gain $K_d = 5.0 \times 10^{-4}$ dampens relative angular velocity. An integral gain of $K_i = 0.01$ accumulates curvature error to enhance suppression of low-frequency oscillations. These gains were selected through a parameter sweep to minimize peak displacement, settling time, and RMS acceleration. To reduce unnecessary control effort once the beam had stabilized, a control shutoff mechanism was introduced: if midpoint displacement remained below 7.5% of the free-response peak for 5 ms, the control law decayed exponentially. This policy ensured efficient actuation while maintaining stability.

4. RESULTS

A finite element model of a fixed-fixed beam was used to simulate its response to impulsive loading, incorporating axial, transverse, and rotational dynamics. Moment-based actuation was applied through a proportional-integral-derivative (PID) controller targeting selected rotational degrees of freedom. To validate the model, a mesh convergence study confirmed adequate spatial resolution, and the conditioning of the integration matrix verified stable time stepping. Static moment loading was also tested to ensure the actuation method produced physically consistent curvature. The following results illustrate the model's accuracy and the effectiveness of PID control in reducing peak displacement, settling time, and RMS acceleration under shock excitation.

4.1. Numerical Validation

To establish the accuracy and numerical reliability of the finite element model, two verification procedures were performed: a mesh convergence analysis and an evaluation of the system conditioning during time integration.

First, a mesh convergence study was performed by analyzing the static response of a fixed-fixed beam subjected to a unit vertical point load at midspan. The vertical displacement at the midpoint was computed using finite element meshes ranging from 10 to 100 elements and compared to the analytical solution from classical Euler-Bernoulli beam theory. As shown in Figure 7, the relative error in midpoint displacement decreased monotonically with increasing mesh density. A discretization of 49 elements (50 nodes) achieved a relative error below 0.1%, indicating excellent agreement with theory while maintaining computational efficiency. This level of accuracy supports the use of a 50-node

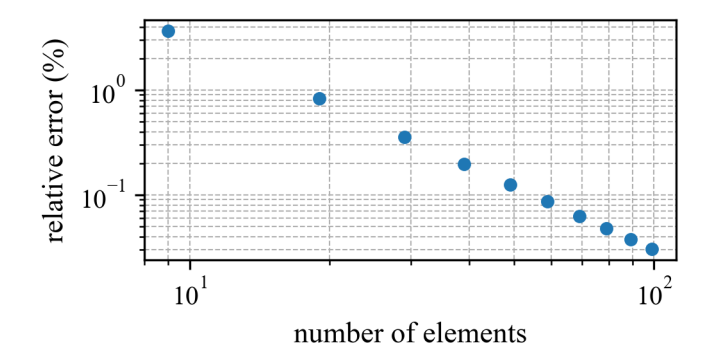


FIGURE 7: THE RELATIVE ERROR IN MIDPOINT DISPLACEMENT VERSUS NUMBER OF ELEMENTS, COMPARED TO THE ANALYTICAL BEAM SOLUTION.

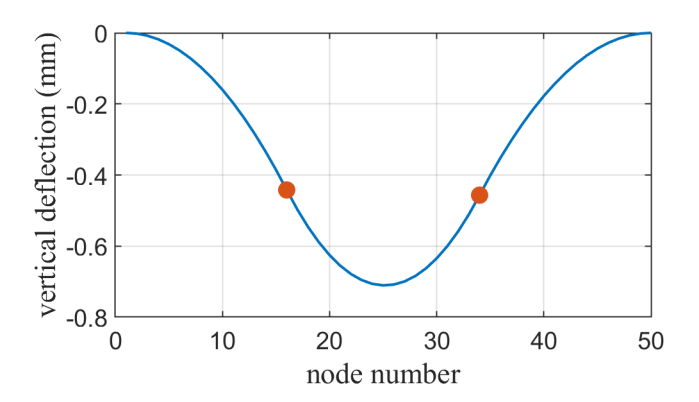


FIGURE 8: THIS FIGURE SHOWS THE STATIC DEFLECTION FROM A MOMENT A COUPLE OF -0.5~NM AT NODE 16 AND +0.5~NM AT NODE 34.

model in dynamic simulations, as further refinement yields diminishing returns. The observed convergence trend aligns with established behavior for Euler-Bernoulli beam elements and confirms the adequacy of the spatial discretization [21].

In addition to verifying spatial accuracy, the numerical stability of the time integration scheme was evaluated by computing the condition number of the effective stiffness matrix $K_{\rm eff}$ used in the Newmark-Beta method. For the 50-node model, the computed condition number was 3.23×10^8 , which, while higher than typical thresholds, remained acceptable for stable time integration due to the moderate system size and consistent numerical performance. In structural dynamics, condition numbers up to 10^8 can be tolerated in double-precision solvers without significant amplification of numerical error, especially when the system matrix is well-scaled [22]. This confirms that the chosen time step and integration method provide stable and accurate results over the simulation window.

4.2. Static Moment-Induced Curvature

A static deflection analysis was conducted to validate the physical behavior of the finite element model when subjected to externally applied moment couples, serving as a baseline check to ensure that localized moments applied at the rotational degrees of

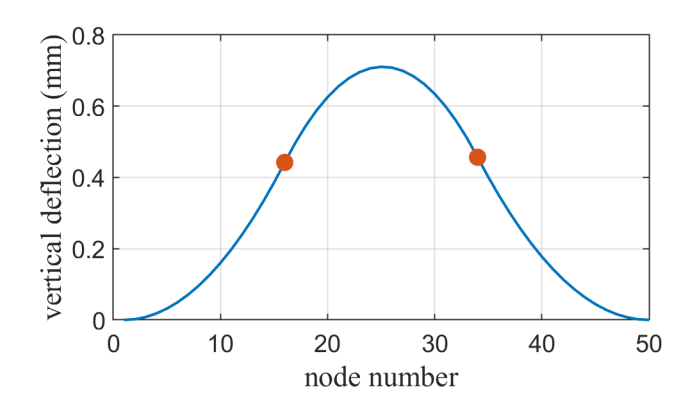


FIGURE 9: THIS FIGURE SHOWS THE STATIC DEFLECTION FROM A REVERSED MOMENT COUPLE OF +0.5 NM AT NODE 16 AND -0.5 NM AT NODE 34.

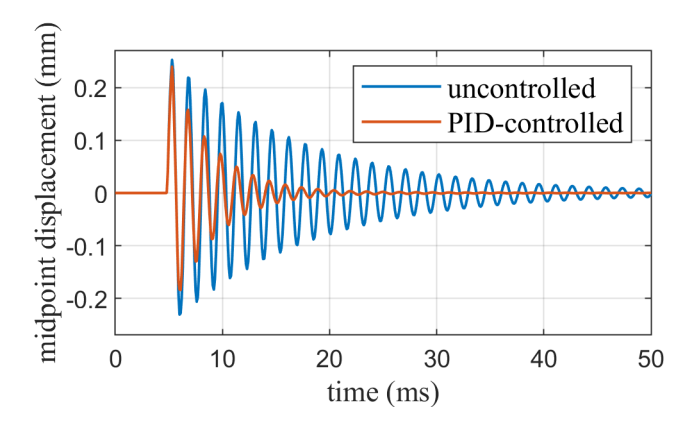


FIGURE 10: THE MIDPOINT DISPLACEMENT OVER TIME FOR BOTH THE FREE AND PID-CONTROLLED CASES.

freedom produce curvature consistent with expected elastic bending behavior in Euler-Bernoulli beam theory and the intended actuation scheme used in the dynamic control simulations.

Two equal and opposite moments of 0.5 Nm were applied at nodes 16 and 34. This magnitude was selected to produce a noticeable yet linear deformation, allowing curvature to be visually assessed without introducing nonlinear geometric effects. The specific node locations were chosen to reflect the same region used for dynamic control, thereby enabling a direct comparison between static and active moment effects.

In the first case, a negative moment was applied on the left and a positive moment on the right. This configuration induced a downward, concave deflection profile, as shown in Figure 8. The resulting curvature confirmed that the finite element formulation correctly interprets moment couples as localized bending loads.

To verify symmetry, the moment signs were reversed: a positive moment was applied on the left and a negative moment on the right. This produced an upward, convex deflection pattern, shown in Figure 9. The resulting deformation was symmetric to the first case but mirrored about the beam's horizontal axis, confirming that the model responds predictably to changes in moment direction.

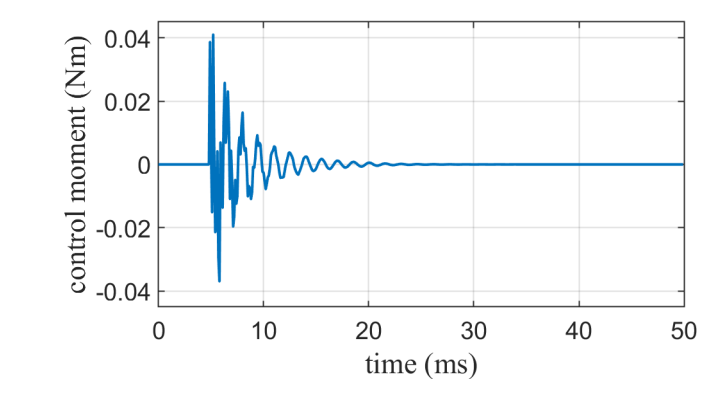


FIGURE 11: THE APPLIED CONTROL MOMENT OVER TIME.

TABLE 2: A PERFORMANCE COMPARISON BETWEEN FREE AND PID-CONTROLLED CASES.

metric	uncontrolled	PID controlled	improvement
peak displacement	0.25 mm	0.24 mm	5.09%
settling time	42.80 ms	16.80 ms	60.75%
RMS acceleration	68.82 dB	68.65 dB	0.25%

4.3. Dynamic Behavior and Control Performance

The dynamic behavior of the fixed-fixed beam was evaluated under impulse loading, with and without active control. The equations of motion were integrated using an ODE solver to simulate the dynamic response under impulsive loading. Figure 10 shows the resulting midpoint displacement histories for the uncontrolled and PID-controlled cases. In the absence of control, the beam experienced a large initial deflection followed by prolonged oscillations dominated by the first bending mode. When the proportional-derivative (PID) controller was activated, the beam settled more rapidly and with lower peak displacement.

The time history of the applied control moment is shown in Figure 11. A high initial torque is applied immediately following the disturbance, followed by a rapid decay as the system stabilizes. This pattern reflects the controller's responsiveness to the transient curvature spike induced by the impulse.

Quantitative performance metrics comparing the two cases are summarized in Table 2. These include peak displacement, settling time, and root mean square (RMS) acceleration at the midpoint, expressed in decibels (dB) to better reflect control performance across magnitudes. The results confirm the effectiveness of moment-based PID control in reducing displacement, settling time, and RMS acceleration.

5. CONCLUSION

This work developed a finite element model simulating the flexural response of fixed-fixed beams under impulsive loading, using moment-based actuation to mimic the effects of piezo-electric devices through localized torque couples. A curvature-, velocity-, and integral-error-based PID control scheme was applied to midspan rotational degrees of freedom, introducing localized damping and correction to suppress vibrations. The model was validated through static deformation and convergence studies, confirming its spatial and temporal accuracy. Compared

to the uncontrolled case, the actively controlled beam exhibited reduced vibration amplitude and a faster return to equilibrium.

Although successful, the model includes simplifying assumptions: Euler-Bernoulli beam theory does not account for geometric nonlinearities; FR4 is assumed isotropic despite being anisotropic; and actuator dynamics, sensor noise, and environmental effects are idealized or omitted. Future work will address these limitations with experimental validation and more realistic actuator modeling. The methods described give a practical foundation for high-rate, model-based vibration control in compact structures with limited actuation authority.

6. ACKNOWLEDGMENTS

This material is based upon algorithms supported by the National Science Foundation grant numbers CCF - 1937535, CCF - 1956071, CCF-2234921, and CPS - 2237696. Additional support from the Air Force Office of Scientific Research (AFOSR) through award no. FA9550-21-1-0083 Any opinions, findings conclusions, or recommendations expressed in this material are those of the authors and do not necessarily reflect the views of the National Science Foundation or the United States Air Force,

REFERENCES

- [1] Verbaan, Cornelis A.M., Peters, Gerrit W.M. and Steinbuch, Maarten. "The advantage of linear viscoelastic material behavior in passive damper design-with application in broadbanded resonance dampers for industrial high-precision motion stages." *Journal of Sound and Vibration* Vol. 386 (2017): pp. 242–250. DOI 10.1016/j.jsv.2016.05.031.
- [2] Dodson, Jacob, Downey, Austin, Laflamme, Simon, Todd, Michael D., Moura, Adriane G., Wang, Yang, Mao, Zhu, Avitabile, Peter and Blasch, Erik. *High-Rate Structural Health Monitoring and Prognostics: An Overview*. Springer International Publishing (2021): pp. 213–217. DOI 10.1007/978-3-030-76004-5 23.
- [3] QI, Rui, WANG, Liang, JIN, Jiamei, YUAN, Lusheng, SHEN, Ziyu and GE, Yuning. "An embedded piezoelectric actuator for active vibration control: Concept, modeling, simulation, and investigation." *Chinese Journal* of Aeronautics Vol. 38 No. 4 (2025): p. 103345. DOI 10.1016/j.cja.2024.103345.
- [4] Ohayon, Rodger. "A unified beam finite element model for extension and shear piezoelectric actuation mechanisms." *Journal of Intelligent Material Systems and Structures* (1997).
- [5] Chandrupatla, Tirupathi R. *Introduction to finite elements in engineering*, fifth edition. ed. Cambridge University Press, Cambridge (2022). Title from publisher's bibliographic system (viewed on 08 Nov 2021).
- [6] Schoeftner, Juergen. "Bending moment tracking and the reduction of the axial stress in vibrating beams by piezoelectric actuation." *Acta Mechanica* Vol. 228 No. 11 (2017): pp. 3827–3838. DOI 10.1007/s00707-017-1918-0.
- [7] Narayanan, S. and Balamurugan, V. "Finite element modelling of piezolaminated smart structures for active vibration control with distributed sensors and actuators." *Journal of*

- *Sound and Vibration* Vol. 262 No. 3 (2003): pp. 529–562. DOI 10.1016/s0022-460x(03)00110-x.
- [8] Wilson, Edward L. *Three dimensional static and dynamic analysis of structures*, 3rd ed. Computers and Structures (1999): Chap. 7, pp. 7–1,7–17.
- [9] Roberts, Trotter, Yount, Ryan, Dodson, Jacob, Moura, Adriane and Downey, Austin R.J. "Towards active structural control strategies for electronic assemblies in high-rate dynamic environments." *94th Shock and Vibration Symposium* (2024).
- [10] ARTS-Lab. "Paper 2025 Finite Element Modeling of Fixed-Fixed Beams Under Shock Excitation with Active Control." GitHub (2025). URL https://github.com/ARTS-Laboratory/Paper-2025-Active-Vibration-Control-of-Fixed-Fixed-Beams-using-Data-driven-Control.
- [11] Yount, Ryan, Roberts, Trotter, Dodson, Jacob, Moura, Adriane and Downey, Austin R.J. "Experimental Analysis to Enable Low-Latency Structural Health Monitoring for Electronics in High-Rate Dynamic Environments." *Springer Nature Switzerland* (2025).
- [12] Rao, Singiresu S. *Mechanical vibrations*, sixth edition in si units, global edition ed. Pearson, Harlow, United Kingdom (2018).
- [13] Legner, D., Wackerfuß, J., Klinkel, S. and Wagner, W. "An advanced finite element formulation for piezoelectric beam structures." *Computational Mechanics* Vol. 52 No. 6 (2013): pp. 1331–1349. DOI 10.1007/s00466-013-0879-y.
- [14] Li, Cong Ying, Zhang, Han Jie and Wang, Dong Dong. "Analysis of Euler-Bernoulli Beam with Piecewise Quadratic Hermite Finite Elements." *Applied Mechanics and Materials* Vol. 444–445 (2013): pp. 163–167. DOI 10.4028/www.scientific.net/amm.444-445.163.

- [15] Soydas, Ozan and Saritas, Afsin. "Free vibration characteristics of a 3d mixed formulation beam element with force-based consistent mass matrix." *Journal of Vibration and Control* Vol. 23 No. 16 (2015): pp. 2635–2655. DOI 10.1177/1077546315619263.
- [16] Chouly, Franz. Finite element approximation of boundary value problems. Compact Textbooks in Mathematics, Birkhäuser, Cham (2025).
- [17] Younis, Mohammad I. and Miles, Ronald. "Response of MEMS Devices Under Shock Loads." *Design Engineering, Parts A and B*: pp. 499–506. 2005. ASMEDC. DOI 10.1115/imece2005-81217.
- [18] Giraldo, Guillermo. "How to Compute the Coefficients for Rayleigh Damping?" SimScale (2021). URL https://www.simscale.com/knowledge-base/rayleigh-damping-coefficients/.
- [19] Crawley, Edward F. and de Luis, Javier. "Use of piezoelectric actuators as elements of intelligent structures." *AIAA Journal* Vol. 25 No. 10 (1987): pp. 1373–1385. DOI 10.2514/3.9792.
- [20] Gibbs, Gary P. and Fuller, Chris R. "Excitation of thin beams using asymmetric piezoelectric actuators." *The Journal of the Acoustical Society of America* Vol. 92 No. 6 (1992): pp. 3221–3227. DOI 10.1121/1.404172.
- [21] Harish, Ajay. "What is Convergence in Finite Element Analysis?" SimScale (2024). URL https://www.simscale.com/blog/convergence-finite-element-analysis/.
- [22] Gavin, Henri P. "Numerical Integration in Structural Dynamics." Course Note (2020). URL https://people.duke.edu/~hpgavin/StructuralDynamics/NumericalIntegration.pdf.